coatings

MDPI

Article

Development of a Controlled Low-Strength Material Containing Paraffin–Rice Husk Ash Composite Phase Change Material

Hongfei Xu and Wenting Qu *

School of City and Architecture Engineering, Zaozhuang University, Zaozhuang 277160, China; xuhongfei2012@163.com
* Correspondence: quwenting1266@126.com

Abstract: In order to reduce heat loss and diffusion of underground heating pipelines, this research incorporated phase change material (PCM) into the controlled low-strength material (CLSM) to prepare a pipeline backfill material with temperature control performance. In response to the problem that PCM leaks easily, a new type of paraffin–rice husk ash composite PCM (PR-PCM) was obtained by adsorbing melted paraffin into rice husk ash. Through mixing PR-PCM with dredged sediment (DS) and ordinary Portland cement (OPC), a controlled low-strength material (CLSM) with temperature control performance was prepared. The flowability, mechanical properties, microscopic characteristics, thermal characteristics, and durability of CLSM were analyzed through flowability, unconfined compressive strength (UCS), X-ray diffraction (XRD), scanning electronic microscopy (SEM), differential scanning calorimetry (DSC), and phase change cycle tests. The results show that when water consumption is constant, as the PR-PCM content increases, the flowability of CLSM increases, and the strength decreases. The CLSM has an obvious paraffin diffraction peak in the XRD pattern, and its microstructure is dense with few pores. The melting point of CLSM is 50.65 °C and the latent heat is 4.10 J/g. Compared with CLSM without PR-PCM, the maximum temperature difference during the heating process can reach 3.40 °C, and the heat storage performance is improved by 4.1%. The strength of CLSM increases and the melting point decreases after phase change cycles. CLSM containing PR-PCM has the characteristics of phase change temperature control, which plays a positive role in reducing heat loss by heating pipelines and temperature change in backfill areas.

Keywords: controlled low-strength material; composite phase change material; engineering performance; microscopic characteristics; thermal properties; durability

check for updates

Citation: Xu, H.; Qu, W. Development of a Controlled Low-Strength Material Containing Paraffin–Rice Husk Ash Composite Phase Change Material. *Coatings* **2024**, *14*, 1173. https://doi.org/10.3390/coatings14091173

Academic Editor: Michel Voué

Received: 20 July 2024
Revised: 4 September 2024
Accepted: 9 September 2024
Published: 11 September 2024

1. Introduction

The increasing costs of heating due to fossil fuel depletion and the resulting emissions of CO_2 and other pollutants have heightened the need for energy conservation and reduced energy consumption in heating systems [1,2]. District intermittent heating has emerged as an efficient method to achieve these objectives [3]. However, district heating requires very long buried pipes to achieve adequate heating coverage, and heat loss due to poor heat insulation of pipelines is inevitable [4]. Heat is conducted through the steel pipes and dissipates to the surrounding soil, negatively impacting the stability of soil temperature [5]. The environmental and safety issues resulting from pipe aging and damage should also not be overlooked. Therefore, it is crucial to develop cost-effective backfill materials with suitable strength that can effectively hinder heat loss while conserving energy and reducing environmental pollution.

Controlled low-strength material (CLSM) is a self-compacted flowable fill cementitious material that can replace traditional compacted backfill soils [6]. CLSM can easily fill narrow areas and is convenient for construction. Its 28-day unconfined compressive strength (UCS) generally falls below 8.3 MPa, and considering later excavation and maintenance, the strength is usually below 2.1 MPa [7]. A large variety of non-standard materials can

be used in CLSM preparation, so there are currently no standard constraints on its mix design. Typically, CLSM consists of sand aggregate, cement, fly ash, and water, with occasional use of other chemical additives [6]. In order to reduce environmental pressure, the application of industrial solid waste in CLSM is also a concern, and the addition of industrial solid waste in CLSM production can reduce production costs at the same time [8]. Xiao et al. [9] prepared cementless CLSM via the reaction of volcanic ash between waste glass powder and hydrated lime, providing an idea for the large-scale utilization of waste glass in construction industries. Chen et al. [10] used five different coal industrial by-products and cement to prepare multi-component coal-based CLSM, which is suitable for structural backfilling with certain strength requirements. When CLSM is used to backfill pipeline excavations, it can make use of soil with undesirable properties. Do et al. [11] produced CLSM using marine dredged soil as a substitute for aggregate and applied it to grouting geothermal systems. Experimental studies revealed that CLSM produced with marine dredged soil and natural sand exhibited high thermal conductivity. Importantly, the bleeding rate of the CLSM mixture prepared with marine dredged soil was much lower than that prepared with ordinary silica sand. However, the strength of CLSM produced using soil as an aggregate is usually not high [12] because soil is easily adsorbed onto the surface of hydration products, hindering deep hydration of cement [13]. Further research has found that the strength of soil-based CLSM mixtures is not only determined by the soil content, but also by the water/cement ratio (w/c), water/solid ratio (w/s), and paste volume ratio (PVR), which also control the development of CLSM properties [1,14,15]. Studies have shown that it is completely feasible to use excavated waste soil to produce CLSM through reasonable proportion design [16]. The utilization of soil-based CLSM for pipeline backfilling is beneficial for reducing project costs and providing significant benefits for sustainable development.

Phase change materials (PCMs), known for their ability to store or release heat during phase transitions, have been widely used in various applications to control heat transfer [17,18]. PCMs offer flexible control of heat transfer and have been widely used in various applications, such as building envelope insulation [19,20] and building energy conservation [21]. Yu et al. [22] applied heat-storage cement mortars containing PCMs to building roofs, providing insights into the efficient use of solar energy in passive buildings. PCM heat storage technology has also been widely concerned with reducing heating and cooling loads. Gencel et al. [23] incorporated composite PCMs into foam concrete to produce building materials with energy storage function. Dora et al. [24] improved the thermal properties of building envelopes by incorporating PCMs into foamed concrete, and the test results showed that PCM wallboard can be used as a high-performance insulation material in the building. Ren et al. [25] mixed microencapsulated PCM into ultra-high-performance concrete to develop a new structure–function integrated concrete with excellent mechanical properties and heat storage properties. The cement slurry containing PCM can effectively solve the instability problem of gas hydrate layers, which is the key obstacle to deep-water cementing. This work supports the safe and efficient exploitation of undersea hydrocarbon resources [26,27]. PCM provides a new solution for hydration heat control of mass concrete. PCM concrete has excellent thermodynamic properties and reduces the risk of temperature increases cracking mass concrete [28,29]. In addition, PCM is also used in road engineering, such as reducing the temperature sensitivity of asphalt pavements [30], improving the thermal performance of asphalt steel bridge decks [31], and easing the thermal curl of concrete rigid pavements [32]. At present, there has been limited research on the temperature control effect of PCMs in backfill materials. Liu et al. [33] added PCM to clay for the construction of earth-rock dams in cold areas, which can improve construction efficiency during cold periods. Dehdezi et al. [34] utilized PCM for soil modification and studied the variation in ground temperature through numerical simulations, finding that PCM-modified soil exhibited a 3 °C reduction in temperature fluctuation compared to traditional soil. Lyne et al. [35] indicated that the addition of PCM effectively reduced soil temperature fluctuations in a region. Yang et al. [36] used various fatty acid-based PCM

to backfill borehole heat exchangers and found that PCM improved the heat exchange efficiency of the exchangers while reducing the soil's thermal interference radius. These findings highlight the significant importance of applying PCM to backfill materials to address heat loss and diffusion in heating pipelines.

However, the state change in PCM during phase transition can easily lead to material leakage, necessitating a method to restrict PCM loss [37,38]. Impregnation is a simple and cost-effective encapsulation method that involves adsorbing PCM into the porous structure of a supporting material to form a stable composite [39]. Porous materials with high porosity and surface area, along with significant capillary and surface tension forces, effectively prevent PCM leakage [40–46]. Common supporting materials include diatomite [47], bentonite [48], ceramsite [49], expanded vermiculite [50], and expanded graphite [51], which possess advantages such as material benefit, stability, and environmental friendliness. To save construction costs and promote environmental protection, solid waste seems to be a more suitable choice as a supporting material. Rice husk ash (RHA) is a waste product generated from the combustion of rice husks. RHA exhibits a large surface area, high porosity, and good adsorption capacity, making it a suitable alternative adsorbent to replace activated carbon [52]. Furthermore, the high silicon content in RHA is considered a supplementary cementitious material with high pozzolanic activity [53,54]. Therefore, RHA can serve as an economical and environmentally friendly supporting material.

In response to heat loss and the influence of heat transfer on the surrounding soil in heating pipelines, PCM (paraffin) was added to CLSM to give it a temperature control function. In order to control the leakage of paraffin during phase transition, a new type of composite phase change material (PR-PCM) was prepared by adsorption of paraffin into rice husk ash, and using it as a partial aggregate for the production of CLSM. Through a series of laboratory tests, the effects of the addition of PR-PCM on the working properties, mechanical properties, microscopic characteristics, thermal characteristics, and durability of CLSM were analyzed. This study will provide a valuable reference for the application of CLSMs containing new composite phase change materials in practical engineering.

2. Materials and Methods

2.1. Raw Materials

The raw materials used in this study for CLSM production included dredged sediment (DS), ordinary portland cement (OPC), rice husk ash (RHA), paraffin, and water. DS was collected from the silt of the Xiaoqing River in Jinan City to realize the resource utilization and reduce encroachment on the surrounding land, and its basic physical properties were determined according to JTG3430-2020 [55], with the results presented in Table 1. The cement used in the experiments was P.O 42.5 OPC produced by a cement company in Zhucheng City, Shandong Province. It had a specific surface area of 358 m^2/kg. RHA, an inorganic porous material, was obtained after high-temperature combustion of rice husks, with SiO_2 being its main chemical component. RHA possesses a distinct fibrous structure, with internal semi-enclosed spaces and surface voids resulting from material stacking. The chemical compositions of DS, OPC, and RHA are presented in Table 2, and the organic matter content of DS is 1.4% by weight.

Table 1. Physical properties of DS.

Physical Properties	Value
Liquid limit (%)	29.2
Plastic limit (%)	22.5
Plasticity index	6.7
Maximum dry density (g/cm^3)	1.93
Optimum water content (%)	14.4

Table 2. The main chemical compositions of DS, RHA, and OPC.

Composition	SiO_2	Al_2O_3	CaO	Fe_2O_3	Na_2O	MgO	K_2O	SO_3
DS	51.10	16.56	13.46	9.73	0.95	2.26	3.95	0.07
OPC	24.99	8.26	51.42	4.03	0.32	3.71	0.88	2.51
RHA	85.83	0.45	1.55	0.23	1.28	1.14	5.19	0.78

Paraffin, selected as the phase change material, was chosen for its high latent heat, low thermal conductivity, chemical stability, excellent thermal stability, and minimal supercooling phenomenon [56]. In this study, Grade 48 fully refined low-temperature paraffin with a melting point of 46 °C to 50 °C was used. Its main chemical formula is C_nH_{2n+2}, and it is a colorless, odorless solid at room temperature. Laboratory tap water was used as the experimental water source.

2.2. Preparation of Paraffin/RHA Composite Material (PR-PCM)

Paraffin, employed as the phase change material, was melted and impregnated into RHA, acting as the supporting material. The mass ratio of paraffin to RHA was set at m(paraffin)/m(RHA) = 2.5. Preliminary experiments indicated that this mass ratio yielded the lowest leakage rate for the composite material. The composite phase change material was shear-crushed and passed through a 5 mm sieve, resulting in the formation of PR-PCM composite material, as shown in Figure 1a. The thermal properties of the composite phase change material were tested using a differential scanning calorimeter, and the results are presented in Figure 1b. It can be observed that the PR-PCM composite material exhibited a phase change onset temperature (T_o) of 26.96 °C (standard deviation σ = 1.36), phase change end temperature (T_c) of 59.73 °C (σ = 2.02), melting point (T_p) of 56.03 °C (σ = 1.85), and latent heat (ΔH) of 94.79 J/g (σ = 1.91).

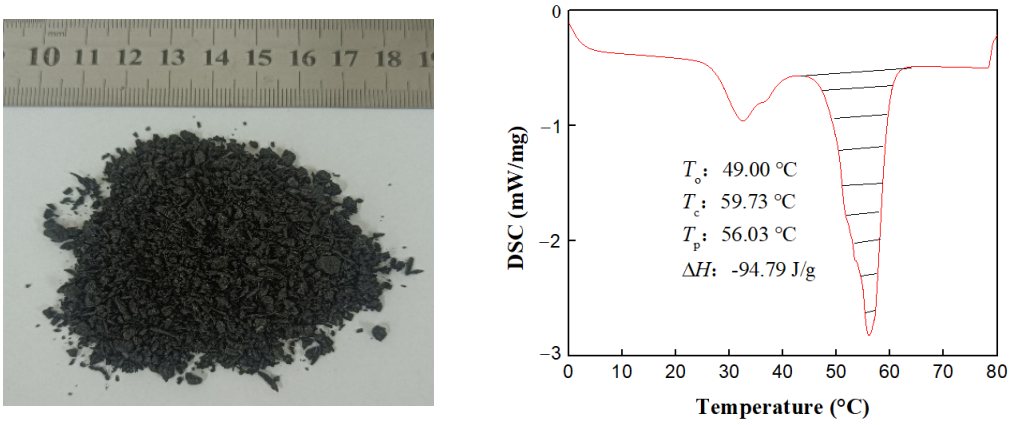

(**a**) (**b**)

Figure 1. PR-PCM (**a**) appearance; (**b**) differential scanning calorimetry (DSC).

2.3. Preparation of CLSM Mixtures

DS and PR-PCM were utilized as fine aggregates, with OPC serving as the cementitious material. All materials were weighed according to the specified mix proportions, ensuring that the fine aggregates passed through a 5 mm sieve. Initially, DS, PR-PCM, and OPC were placed into a cement mixer (JJ-5, Guanghui test instrument Co., Ltd., Cangzhou, China) and dry-mixed for 30 s to ensure uniform blending. Subsequently, the calculated amount of water was added to the mixer, and the mixture was further stirred for 2 min. The well-mixed mixture was poured into a 70.7 mm × 70.7 mm × 70.7 mm cubic mold. Due to the self-leveling and self-compacted nature of CLSM mixtures, no additional vibration was required during pouring. After pre-curing for 24 h at room temperature, the specimens

were de-molded and labeled, then placed in a curing box for the specified testing age. The curing temperature was set at 20 °C, with a humidity of 97%.

2.4. Testing Program

In this study, CLSM was prepared by varying the content of PR-PCM. DS is partially replaced by PR-PCM as a fine aggregate. The PR-PCM content was determined using the equal volume replacement method, where the PR-PCM content was equaled to the volume ratio of PR-PCM to DS (PR-PCM content = $V_{PR\text{-}PCM}/V_{DS}$). Initially, while keeping the water content constant, the PR-PCM content was changed to obtain mixtures labeled D100P0, D90P10, D80P20, and D70P30. Subsequently, by adjusting the water content of the mixtures to match the flowability of D100P0, additional mixtures labeled D90P10B, D80P20B, and D70P30B were prepared. The CLSM mix proportions are presented in Table 3. The CLSM mixtures with different proportions were subjected to tests, including flowability, unconfined compressive strength (UCS), X-ray diffraction (XRD), scanning electron microscopy (SEM), differential scanning calorimetry (DSC), and phase change cycle. The overall experimental design is illustrated in Figure 2.

Table 3. Mix proportions for CLSM mixtures.

Mixture Name	PR-PCM Content (%)	Weight Fraction			
		Water	DS	OPC	PR-PCM
D100P0	0	2.9	5.0	1	0
D90P10	10	2.9	4.5	1	0.2
D80P20	20	2.9	4.0	1	0.4
D70P30	30	2.9	3.5	1	0.5
D90P10B	10	2.7	4.5	1	0.2
D80P20B	20	2.4	4.0	1	0.4
D70P30B	30	2.2	3.5	1	0.5

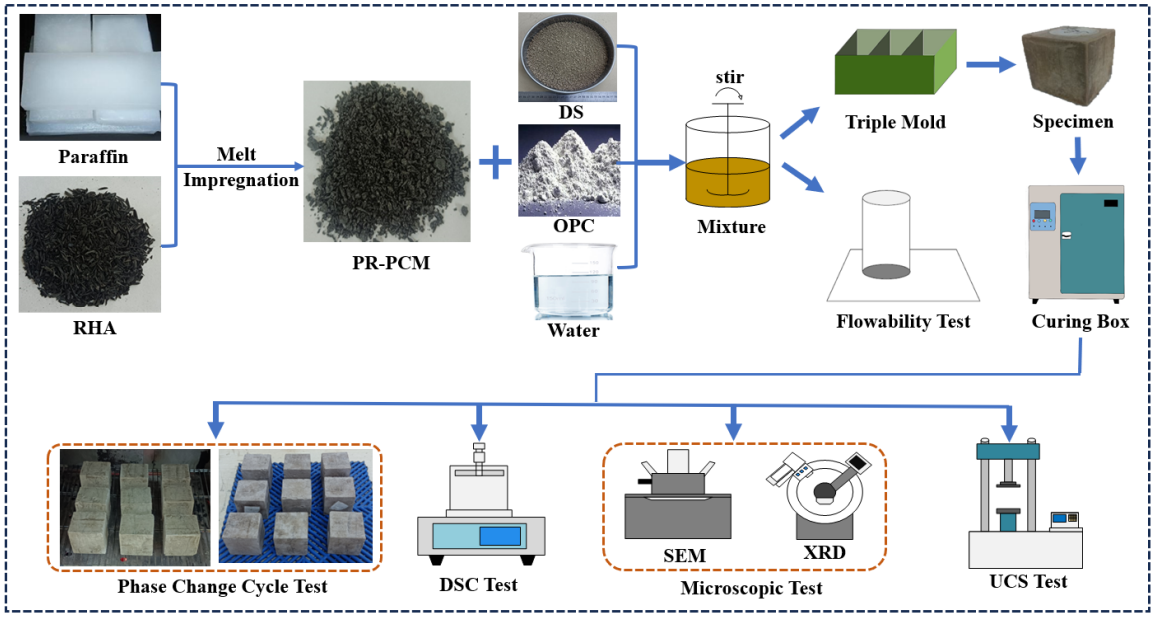

Figure 2. Overall testing program.

2.5. Testing Methods

2.5.1. Flowability Test

The flowability of CLSM was tested using the pipe flow method according to ASTM D 6103 [57]. The test apparatus consisted of a hollow cylinder with a height of 150 mm and an inner diameter of 75 mm. Freshly mixed CLSM was poured into the cylinder until it was

completely filled, and then the cylinder was quickly lifted vertically upwards to allow the mixture to freely spread on a glass plate. When the spreading of the mixture stopped, the diameter was measured, and the average of two measurements was taken as the flowability of the mixture.

2.5.2. Unconfined Compressive Strength (UCS) Test

The UCS test of CLSM was performed in accordance with JGJ/T 70-2009 [58]. The specimens were cured for 3, 7, and 28 days. The test was conducted using a pavement material strength tester (LD127, Guanghui test instrument Co., Ltd., Cangzhou, China) with the load plate moving upward at a rate of 1 mm/min until the specimen failed. The average compressive strength of three specimens was calculated as the test result.

2.5.3. X-ray Diffraction (XRD) Test

X-ray diffraction (XPert PRO, PANalytical B.V., EA Almelo, Holland) was employed to analyze the phase composition of CLSM. Samples were taken from crushed blocks after the UCS test at 28 days and ground into dry powder passing through a 0.075 mm sieve. The scanning range was set from 10° to 80° at a scanning rate of 10°/min.

2.5.4. Scanning Electronic Microscopy (SEM) Test

SEM (Supra55, Carl Zeiss AG, Oberkochen, Germany) was utilized to observe the microstructure of CLSM using a scanning electronic microscope. Samples were taken from crushed blocks after the UCS test at 28 days and cut into 10 mm × 5 mm × 5 mm specimens. Due to the poor conductivity of the scanning samples, a gold sputtering treatment was applied to the surface of the samples to ensure optimal scanning electron microscopy results. The samples were fixed onto the testing stage using conductive adhesive for scanning testing.

2.5.5. Differential Scanning Calorimetry (DSC) Test

DSC was conducted to measure the thermal properties of CLSM cured for 28 days using a DSC instrument (DSC 3, Mettle-Toledo, Zurich, Switzerland). The test samples were crushed specimens obtained after the UCS test. The test was conducted in a nitrogen atmosphere, with a heating rate of 10 K/min. The sample mass used for testing was approximately 10 mg. Additionally, a temperature sensor (NTC (10 K/3435), temperature range of 50 °C to 110 °C) was placed at the center of the specimen, which was cured for 28 days after demolding. The test specimen was heated by a constant temperature heat source at 80 °C to study the thermal control performance of PR-PCM in CLSM.

2.5.6. Phase Change Cycle Test

To investigate the long-term performance of CLSM containing PR-PCM, a phase change cycle test was conducted. Once the specimens were cured for 28 days, they were placed in a drying oven at 40 °C for 72 h. After drying, the specimens were further heated to 80 °C and kept for 8 h in the oven. Subsequently, the specimens were cooled to room temperature and kept for 16 h in a dry sealed box. These two processes constituted one cycle of phase change. UCS and DSC tests were conducted on specimens that had undergone 0, 3, 6, and 9 cycles of phase change.

In order to ensure the quality of test data, 3 parallel specimens were selected for each group of different types of tests and the final results were averaged.

3. Results and Discussion

3.1. Flowability Analysis

The flowabilities of CLSM mixtures with different proportions are shown in Figure 3. It can be observed that, at a constant water content, the flowability of the mixture increases with the increase in PR-PCM content. The water absorption of materials in the mixture affects its flowability, and DS has a smaller particle size and relatively larger specific

surface area, resulting in more water adsorption on its surface. Therefore, achieving the target flowability requires more water [13]. However, when PR-PCM is used as a volume replacement for DS, the water demand of the mixture decreases, leading to an increase in flowability. D90P10B, D80P20B, and D70P30B require different amounts of water to achieve the same target flowability. With the decrease in water content, the reduction in the flowability of CLSM mixtures becomes significant. According to ACI 229R-13 [7], the flowability of CLSM mixtures should be controlled between 200 mm and 300 mm. Excessive flowability can lead to the segregation of components, severely affecting mechanical and other properties of the mixture.

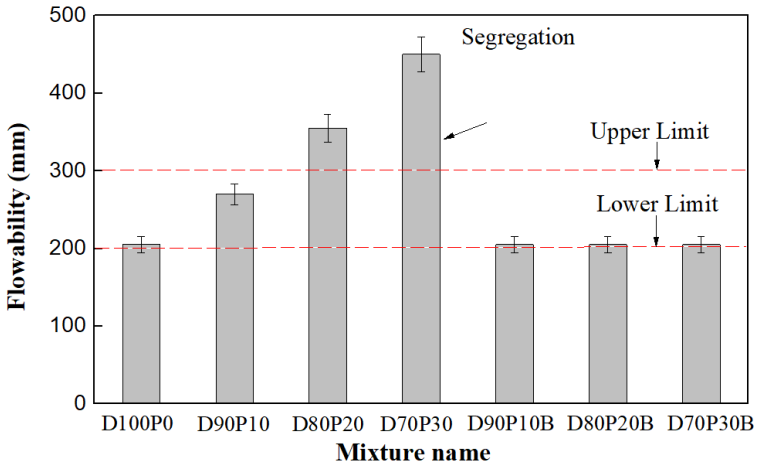

Figure 3. Flowability of different CLSM mixtures.

3.2. UCS Analysis

The UCS of CLSM mixtures with different proportions at 3 days, 7 days, and 28 days is shown in Figure 4. It can be observed that, at the 3-day curing period, the strengths of D90P10, D80P20, and D70P30 are reduced by 33.3%, 42.6%, and 38.9%, respectively, compared to D100P0. At the 7-day curing period, the strength of CLSM is reduced by 9.8%, 35.4%, and 42.7%, respectively. At the 28-day curing period, the strength of CLSM is reduced by 5.8%, 17.4%, and 33.5%, respectively. At a constant water content, the strengths at each curing period decrease with the increase in PR-PCM content. This is because PR-PCM is an organic material, while DS and cement are inorganic materials, and with the increase in PR-PCM content, the air void content in the cementitious matrix increases, adversely affecting the mechanical properties of CLSM [25].

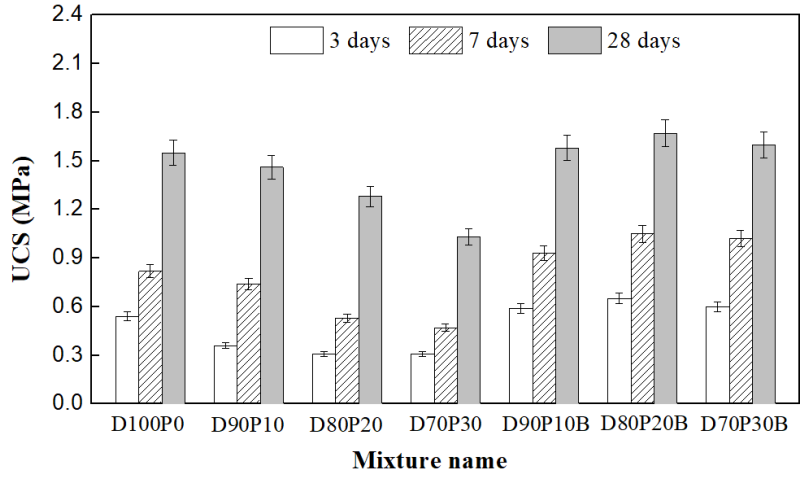

Figure 4. UCS of different CLSM mixtures.

When the water content is reduced to control the consistent flowability of the mixture, D90P10B, D80P20B, and D70P30B exhibit significant strength improvements compared to D90P10, D80P20, and D70P30. This indicates that variations in water content have a significant impact on the strength of the mixture.

3.3. XRD Spectrum Analysis

Based on the test results of flowability and strength, and considering their engineering performance, D80P20B, which has a high PR-PCM content and the highest strength, was selected for the microscopic characterization analysis, with D100P0 serving as the control group.

The XRD spectra of D100P0 and D80P20B at 28 days are shown in Figure 5. It can be observed that, compared to D100P0, there is a distinct peak corresponding to paraffin wax in D80P20B. The presence of the paraffin wax diffraction peak indicates that the CLSM containing PR-PCM exhibits phase change characteristics. It also suggests that the presence of PR-PCM in the hydration process of the mixture at 28 days has minimal influence on the hydration of cement. The detection of quartz, calcite, and feldspar in the CLSM indicates the presence of these minerals. The hydration products at 28 days primarily consist of C-S-H, AFt, and AFm phases. In the early hydration stage of OPC, AFt is the predominant product. Due to the lower sulfur content in CLSM, the transformation from AFt to AFm occurs gradually in the later stages of hydration.

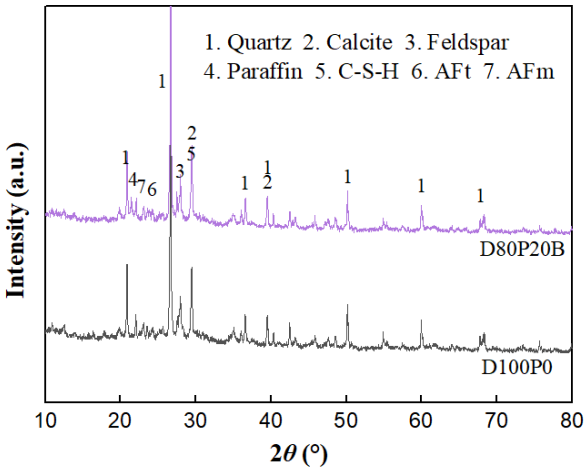

Figure 5. XRD patterns of CLSM mixtures.

3.4. SEM Analysis

The SEM results of D100P0 and D80P20B at 28 days are shown in Figure 6, with an image magnification of 2000. In the images, gel-like C-S-H, needle-like AFt, and plate-like AFm can be observed. While AFt and AFm play a certain role in the strength of the specimens, their presence in large quantities can have a detrimental effect on the strength due to their expansive nature. C-S-H, on the other hand, acts as the key provider of strength by bonding and filling the soil particles to construct the main framework.

In Figure 6a, a larger number of soil particles and relatively larger voids can be observed, indicating poor cohesion between the internal substances of the specimen. Due to the higher water content in D100P0, the presence of water weakens the adhesive ability of C-S-H gel to the DS particles, and the evaporation of water within the specimen creates more voids. Additionally, due to the lower reactivity of the dredged sediment, the cement hydration products have poor adhesion to the soil particles in D100P0. This also contributes to the more pronounced microstructure porosity observed in D100P0, which is primarily made of dredged sediment as the main aggregate. In Figure 6b, a larger amount of C-S-H gel can be seen adhering to and filling the voids among the internal substances of

the specimen. Furthermore, the reduction in water content improves the compactness of D80P20B.

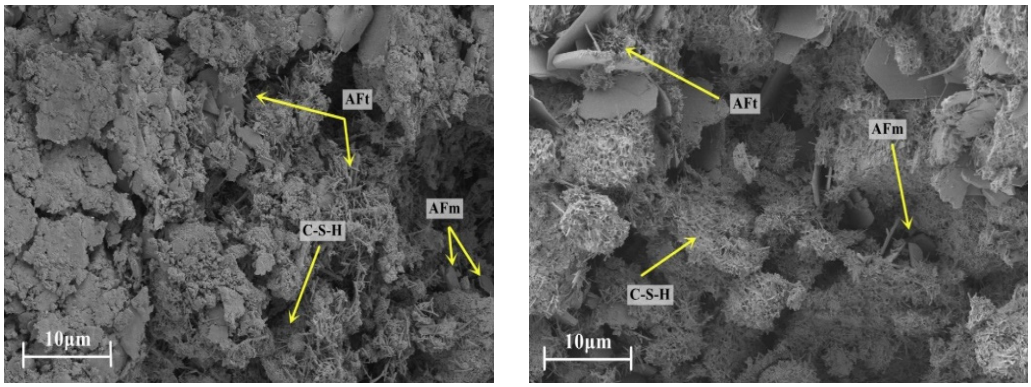

(**a**) (**b**)

Figure 6. SEM images of CLSM mixtures (**a**) D100P0 and (**b**) D80P20B.

3.5. DSC Analysis

The DSC curve of D80P20B after 28 days of curing is shown in Figure 7. It can be observed that D80P20B exhibits phase transition behavior. The melting point (T_p) of the D80P20B mixture is determined to be 50.65 °C, with a latent heat (ΔH) of 4.10 J/g. Compared to PR-PCM, D80P20B demonstrates an earlier T_p, allowing it to exhibit its temperature control performance at an earlier stage. This characteristic is advantageous for the practical application of backfill materials in engineering projects [22].

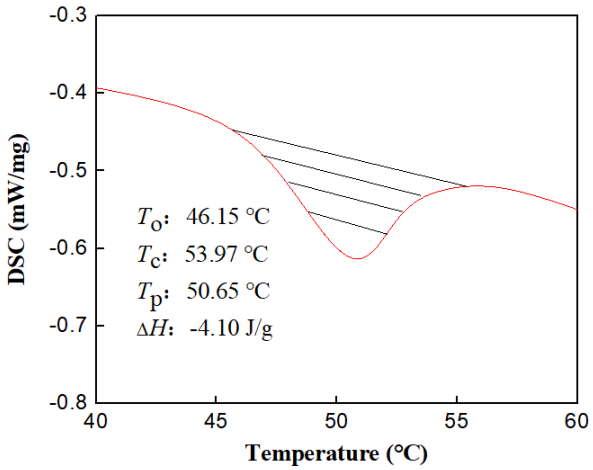

Figure 7. DSC curve of D80P20B.

Placing a temperature sensor inside the cubic specimen of D80P20B and D100P0 (Figure 8) gave the temperature profiles within the specimens over time (Figure 9). From Figure 9, it can be observed that the temperature difference between D80P20B and D100P0 initially increases and then decreases over time due to the presence of PR-PCM. The maximum temperature difference of 3.4 °C is reached at 39 min of heating. Subsequently, the temperature difference between the two groups of specimens decreases with increasing heating time. This phenomenon can be attributed to the limited content of PR-PCM in the mixture. It is evident that incorporating PR-PCM into CLSM can effectively reduce the influence of thermal diffusion on the backfill material.

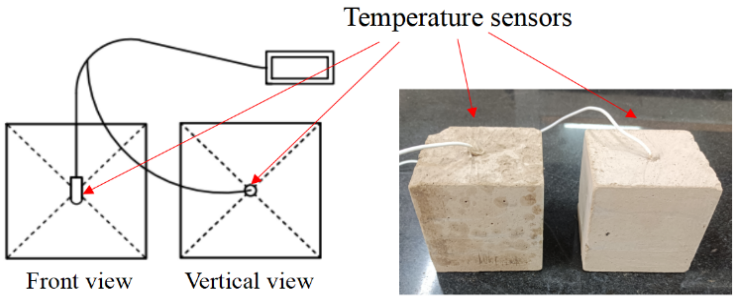

Figure 8. Layout of temperature sensors.

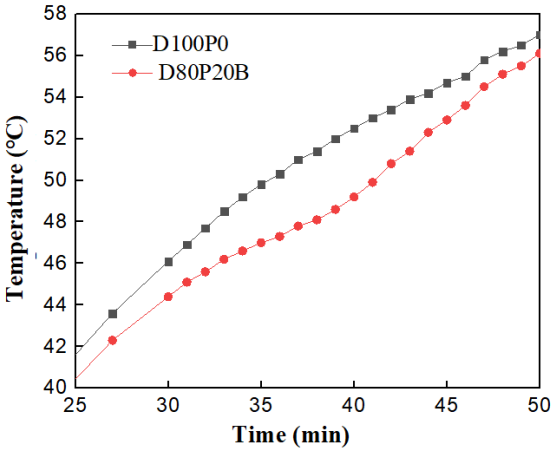

Figure 9. Temperature curves.

3.6. Thermal Storage Performance Analysis

Specific heat capacity is a crucial parameter for characterizing the thermal properties of phase change materials. A higher specific heat capacity indicates that the material can absorb or release more heat per unit mass as its temperature increases or decreases, indicating better thermal storage and release performance. The specific heats of materials in CLSM were measured by the specific heat measuring instrument (TF-BRA, Nanjing Wanhe Co., Ltd., Nanjing, China), as shown in Table 4. According to Table 4, the specific heat capacity of specimen D100P0 is calculated to be 2056 J/(kg·°C), while the specific heat capacity of D80P20B is 2140 J/(kg·°C). It can be observed that the addition of PR-PCM effectively enhances the thermal properties of CLSM. Moreover, to investigate the thermal storage capacity of CLSM with PR-PCM, the heat absorbed by the materials during the period when the temperatures of the two groups of specimens reach equilibrium, as shown in Figure 9, is calculated. The heat absorbed by D100P0 and D80P20B is calculated based on Equation (1). The theoretical heat absorbed per unit mass of D100P0 is 71,540 J, while that of D80P20B is 74,473 J. Compared to ordinary CLSM, CLSM with PR-PCM exhibits a 4.1% improvement in thermal storage performance. The calculation results demonstrate that the addition of PR-PCM to CLSM can effectively enhance the thermal storage capacity of the mixture, reducing heat loss and diffusion in heating supply pipelines.

$$Q = C \times M \times \Delta T \quad (1)$$

Q: The heat absorbed or released by materials;
C: Specific Heat;
M: The weight of materials;
ΔT: The changing temperature of materials.

Table 4. The specific heat of materials in CLSM.

Material	Water	DS	OPC	PR-PCM
Specific Heat ($J \cdot kg^{-1} \cdot °C^{-1}$)	4200	1057	840	1790

3.7. Phase Change Cycle Analysis

The USC and DSC test results of D80P20B under different numbers of phase change cycles are presented in Table 5. As the number of phase change cycles increases, the strength of the specimens gradually increases. After three cycles, the strength of the specimens approaches the maximum excavation strength limit, and after nine cycles, the strength increases by approximately 1.5 times compared to the initial state. The change in specimen strength is attributed to the evaporation of water content and the transfer of paraffin, which is another important factor.

Table 5. USC and DSC test results under different numbers of phase change cycles.

Number of Phase Change Cycles (N)	UCS (MPa)	T_o (°C)	T_c (°C)	T_p (°C)	ΔH (J/g)
0	1.85	46.15	53.97	50.65	4.10
3	2.10	43.12	53.72	50.04	5.71
6	2.43	41.31	53.59	48.83	5.14
9	2.51	41.19	51.98	47.75	3.32

The phase change onset temperature (T_o), phase change end temperature (T_c), and melting point (T_p) decrease with increasing number of phase change cycles. Initially, there is no leakage of paraffin from the specimens. However, after experiencing phase change cycles, some paraffin in the specimens undergoes transfer, resulting in an expanded phase change region. Consequently, the latent heat (ΔH) of the specimens increases after three and six cycles compared to 0 cycles (initial state). However, after the ninth phase change cycle, the latent heat of the specimens decreases. This decrease is because after multiple phase change cycles, there is transfer and partial loss of paraffin, leading to a decrease in the paraffin content per unit mass compared to the initial state. Based on the above test results, it can be concluded that some paraffin in PR-PCM is lost after repeated "solid–liquid" phase change cycles. When flowing through the particles, it exhibits its own binding properties, bonding the particles together to form a mixture, thereby reducing the porosity of the specimens and improving the macroscopic strength.

4. Conclusions

In this study, a composite phase change material (PR-PCM) was developed using RHA and paraffin through a heating immersion process. The CLSM with temperature control performance was created by mixing PR-PCM with DS, cement, and water. The main conclusions are as follows:

(1) The properties of the CLSM mixture were significantly influenced by the PR-PCM content. As the volume ratio of PR-PCM/DS increased, the flowability of the mixture increased while the strength decreased. When the PR-PCM content was constant but the water content was decreased, the flowability decreased while the strength increased.
(2) XRD analysis of the CLSM containing PR-PCM revealed the presence of paraffin diffraction peaks, which indicated that PR-PCM can exist stably in CLSM during the hydration process of the mixture. The micro-scale compactness of the mixture reflects its macro-scale strength. The decrease in water consumption increased the micro density and strength of the mixture.
(3) The melting point of CLSM containing PR-PCM was lower than that of PR-PCM, which allowed the mixture to exhibit its temperature control performance at an earlier

stage. The temperature difference between CLSM containing PR-PCM and ordinary CLSM could reach 3.4 °C, indicating that CLSM containing PR-PCM has better heat storage performance and can effectively reduce heat diffusion.

(4) The CLSM containing PR-PCM exhibited good durability and met the long-term strength requirements. After undergoing phase change cycles, the strength increased and the melting point decreased. The adsorption of rice husk ash and hydration products effectively reduced paraffin leakage.

Although the addition of PR-PCM affects the working performance and mechanical properties of CLSM, it has better temperature control and heat storage performance and can effectively reduce heat diffusion. Especially for intermittent intelligent heating systems, using the latent heat of PCM in the process of phase change to achieve heat storage or release is a good way of preventing heat loss. This research is of great significance for realizing the sustainable development goal of energy conservation and environmental protection. It is worth noting that the conclusions reached in this paper are based on the results of laboratory tests and have not been verified by actual engineering, so it is necessary to carry out field tests to investigate the practical application effect of the new heating pipeline backfill material.

Author Contributions: Conceptualization, H.X. and W.Q.; methodology, H.X.; validation, W.Q.; formal analysis, H.X.; investigation, H.X.; resources, H.X.; data curation, H.X.; writing original draft, H.X. and W.Q.; writing review, W.Q.; supervision, W.Q. All authors have read and agreed to the published version of the manuscript.

Funding: This research received no funding.

Institutional Review Board Statement: Not applicable.

Informed Consent Statement: Not applicable.

Data Availability Statement: The data presented in this study are available on request from the corresponding author.

Conflicts of Interest: The authors declare no conflicts of interest.

Abbreviations and Nomenclature

CLSM	Controlled low-strength material
PCM	Phase change material
PR	Paraffin–Rice husk ash
PR-PCM	Paraffin–Rice husk ash composite phase change material
DS	Dredged sediment
OPC	Ordinary Portland cement
UCS	Unconfined compressive strength
XRD	X-ray diffraction
SEM	Scanning electronic microscopy
DSC	Differential scanning calorimetry
PVR	Paste volume ratio
RHA	Rice husk ash
C-S-H	Calcium silicate hydrate
T_o	Phase change onset temperature
T_c	Phase change end temperature
T_p	Melting point
ΔH	Latent heat
σ	Standard deviation

References

1. Kecebas, A.; Alkan, M.A.; Bayhan, M. Thermo-economic analysis of pipe insulation for district heating piping systems. *Appl. Therm. Eng.* **2011**, *31*, 3929–3937. [CrossRef]
2. Liiv, J.; Teppand, T.; Rikmann, E.; Tenno, T. Novel ecosustainable peat and oil shale ash-based 3D-printable composite material. *Sustain. Mater. Technol.* **2018**, *17*, e00067. [CrossRef]
3. Wang, Z.; Luo, M.; Geng, Y.; Lin, B.; Zhu, Y. A model to compare convective and radiant heating systems for intermittent space heating. *Appl. Energy* **2018**, *215*, 211–226. [CrossRef]
4. Hirsch, P.; Duzinkiewicz, K.; Grochowski, M.; Piotrowski, R. Two-phase optimizing approach to design assessments of long distance heat transportation for CHP systems. *Appl. Energy* **2016**, *182*, 164–176. [CrossRef]
5. Dalla-Rosa, A.; Li, H.; Svendsen, S. Method for optimal design of pipes for low-energy district heating with focus on heat losses. *Energy* **2011**, *36*, 2407–2418. [CrossRef]
6. Kong, X.; Wang, G.; Rong, S.; Liang, Y.; Liu, M.; Zhang, Y. Utilization of fly ash and red mud in soil-based controlled low strength materials. *Coatings* **2023**, *13*, 893. [CrossRef]
7. *ACI 229R*; Controlled Low-Strength Materials. American Concrete Institute: Farmington Hill, MI, USA, 2013.
8. Kaliyavaradhan, S.K.; Ling, T.C.; Guo, M.Z. Upcycling of wastes for sustainable controlled low-strength material: A review on strength and excavatability. *Environ. Sci. Pollut. Res.* **2022**, *29*, 16799–16816. [CrossRef]
9. Xiao, R.; Polaczyk, P.; Jiang, X.; Zhang, M.; Wang, Y.; Huang, B. Cementless controlled low-strength material (CLSM) based on waste glass powder and hydrated lime: Synthesis, characterization and thermodynamic simulation. *Constr. Build. Mater.* **2021**, *275*, 122157. [CrossRef]
10. Chen, T.; Yuan, N.; Wang, S.; Hao, X.; Zhang, X.; Wang, D.; Yang, X. The effect of bottom ash ball-milling time on properties of controlled low-strength material using multi-component coal-based solid wastes. *Sustainability* **2022**, *14*, 9949. [CrossRef]
11. Do, T.M.; Do, A.N.; Kang, G.O.; Kim, Y.S. Utilization of marine dredged soil in controlled low-strength material used as a thermal grout in geothermal systems. *Constr. Build. Mater.* **2019**, *21*, 613–622. [CrossRef]
12. Chittoori, B.; Puppala, A.J.; Raavi, A. Strength and stiffness characterization of controlled low-strength material using native high-plasticity clay. *J. Mater. Civ. Eng.* **2014**, *26*, 04014007. [CrossRef]
13. Qian, J.; Hu, Y.; Zhang, J.; Xiao, W.; Ling, J. Evaluation the performance of controlled low strength material made of excess excavated soil. *J. Clean. Prod.* **2019**, *214*, 79–88. [CrossRef]
14. Alizadeh, V. New approach for proportioning of controlled low strength materials. *Constr. Build. Mater.* **2019**, *201*, 871–878. [CrossRef]
15. Huang, M.; Huang, C.; Lin, J.; Ho, M. Investigated on predictive compressive strength model and setting time of controlled low-strength materials. *Int. J. Pavement Res. Technol.* **2020**, *13*, 129–137. [CrossRef]
16. Sheen, Y.N.; Zhang, L.H.; Le, D.H. Engineering properties of soil-based controlled low-strength materials as slag partially substitutes to Portland cement. *Constr. Build. Mater.* **2013**, *48*, 822–829. [CrossRef]
17. Chandel, S.S.; Agarwal, T. Review of current state of research on energy storage, toxicity, health hazards and commercialization of phase changing materials. *Renew. Sustain. Energy Rev.* **2017**, *67*, 581–596. [CrossRef]
18. Kant, K.; Biwole, P.H.; Shamseddine, I.; Tlaiji, G.; Pennec, F.; Fardoun, F. Recent advances in thermophysical properties enhancement of phase change materials for thermal energy storage. *Sol. Energy Mater. Sol. Cells* **2021**, *231*, 111309. [CrossRef]
19. Kurdi, A.; Almoatham, N.; Mirza, M.; Ballweg, T.; Alkahlan, B. Potential phase change materials in building wall construction—A review. *Materials* **2021**, *14*, 5328. [CrossRef]
20. Zou, T.; Xu, T.; Cui, H.; Tao, H.; Xu, H.; Zhou, X.; Chen, Q.; Chen, J.; Huang, G.; Sun, Y. Super absorbent polymer as support for shape-stabilized composite phase change material containing $Na_2HPO_4{\cdot}12H_2O$–$K_2HPO_4{\cdot}3H_2O$ eutectic hydrated salt. *Sol. Energy Mater. Sol. Cells* **2021**, *231*, 111334. [CrossRef]
21. Wang, P.; Liu, Z.; Zhang, X.; Hu, M.; Zhang, L.; Fan, J. Adaptive dynamic building envelope integrated with phase change material to enhance the heat storage and release efficiency: A state-of-the-art review. *Energy Build.* **2023**, *286*, 112928. [CrossRef]
22. Yu, K.; Liu, Y.; Jia, M.; Wang, C.; Yang, Y. Thermal energy storage cement mortar containing encapsulated hydrated salt/fly ash cenosphere phase change material: Thermo-mechanical properties and energy saving analysis. *J. Energy Storage* **2022**, *51*, 104388. [CrossRef]
23. Gencel, O.; Ustaoglu, A.; Benli, A.; Hekimoglu, G.; Sari, A.; Erdogmus, E.; Sutcu, M.; Kaplan, G.; Bayraktar, O. Investigation of physico-mechanical, thermal properties and solar thermoregulation performance of shape-stable attapulgite based composite phase change material in foam concrete. *Sol. Energy* **2022**, *236*, 51–62. [CrossRef]
24. Dora, S.; Barta, R.; Mini, K. Study on foam concrete incorporated with expanded vermiculite/capric acid PCM-A novel thermal storage high-performance building material. *Constr. Build. Mater.* **2023**, *392*, 131903. [CrossRef]
25. Ren, M.; Wen, X.; Gao, X.; Liu, Y. Thermal and mechanical properties of ultra-high performance concrete incorporated with microencapsulated phase change material. *Constr. Build. Mater.* **2021**, *273*, 121714. [CrossRef]
26. Yang, G.; Lei, G.; Liu, T.; Zheng, S.; Qu, B.; Que, C.; Feng, Y.; Jiang, G. Development and application of low-melting-point microencapsulated phase change materials for enhanced thermal stability in cementing natural gas hydrate layers. *Geoenergy Sci. Eng.* **2024**, *238*, 212846. [CrossRef]
27. Cai, J.; Zhou, J.; Liu, C.; Mei, K.; Zhang, C.; Cheng, X. Microencapsulated phase change material-cement composites for cementing the natural gas hydrate layer. *Constr. Build. Mater.* **2023**, *399*, 132591. [CrossRef]

28. Wang, Y.; Wang, C.; Luo, A.; Dong, M.; Su, Q.; Zhou, C.; Zhang, Z.; Pei, Y. Experimental Investigation on a Novel Temperature-Controlled Phase Change Aggregate Concrete: Thermo-Mechanical Properties and Hydration Heat Control. *Materials* **2023**, *16*, 5269. [CrossRef]
29. Wang, L.; Wang, L.; Ju, S.; Miao, Y.; Wang, Y.; Wang, F.; Sui, S.; Jiang, J. Study on design, preparation, and performance of low-temperature rising concrete with energy storage aggregate. *Struct. Concr.* **2023**, *24*, 6539–6551. [CrossRef]
30. Cheng, C.; Liu, J.; Gong, F.; Fu, Y.; Cheng, X.; Qiao, J. Performance and evaluation models for different structural types of asphalt mixture using shape-stabilized phase change material. *Constr. Build. Mater.* **2023**, *383*, 131411. [CrossRef]
31. Hu, H.; Chen, W.; Cai, X.; Xu, T.; Cui, H.; Zhou, X.; Chen, J.; Huang, G.; Sun, Y. Study on preparation and thermal performance improvements of composite phase change material for asphalt steel bridge deck. *Constr. Build. Mater.* **2021**, *310*, 125255. [CrossRef]
32. Liao, W.; Zeng, C.; Zhuang, Y.; Ma, H.; Deng, W.; Huang, J. Mitigation of thermal curling of concrete slab using phase change material: A feasibility study. *Cem. Concr. Compos.* **2021**, *120*, 104021. [CrossRef]
33. Liu, D.; Wang, Y.; Liang, J. Potential Applications of Phase Change Materials to Extend the Winter Construction Time of Earth-Rock Dam in Cold Regions. *J. Mater. Civ. Eng.* **2021**, *33*, 04021194. [CrossRef]
34. Dehdezi, P.K.; Hall, M.R.; Dawson, A.R. Enhancement of soil thermo-physical properties using microencapsulated phase change materials for ground source heat pump applications. *Appl. Mech. Mater.* **2012**, *110–116*, 1191–1198. [CrossRef]
35. Lyne, Y.; Paksoy, H.; Farid, M. Laboratory investigation on the use of thermally enhanced phase change material to improve the performance of borehole heat exchangers for ground source heat pumps. *Int. J. Energy Res.* **2019**, *43*, 4148–4156. [CrossRef]
36. Yang, W.; Xu, R.; Yang, B.; Yang, J. Experimental and numerical investigations on the thermal performance of a borehole ground heat exchanger with PCM backfill. *Energy* **2019**, *174*, 216–235. [CrossRef]
37. Shen, Y.; Liu, S.; Zeng, C.; Zhang, Y.; Li, Y.; Han, X.; Yang, L.; Yang, X. Experimental thermal study of a new PCM-concrete thermal storage block (PCM-CTSB). *Constr. Build. Mater.* **2021**, *293*, 123540. [CrossRef]
38. Yoo, D.; Jeon, I.; Woo, B.; Kim, H. Performance of energy storage system containing cement mortar and PCM/epoxy/SiC composite fine aggregate. *Appl. Therm. Eng.* **2021**, *198*, 117445. [CrossRef]
39. Zhang, P.; Cheng, Z.; Chen, Z.; Gao, Y. Oleophobic modification of clay minerals to improve encapsulation ratios of shape-stabilized phase change materials: A universal method. *Prog. Nat. Sci-Mater.* **2021**, *31*, 904–910. [CrossRef]
40. Zhang, P.; Cui, Y.; Zhang, K.; Wu, S.; Chen, D.; Gao, Y. Enhanced thermal storage capacity of paraffin/diatomite composite using oleophobic modification. *J. Clean. Prod.* **2021**, *279*, 123211. [CrossRef]
41. Liu, Y.; Sun, F.; Yu, K.; Yang, Y. Experimental and numerical research on development of synthetic heat storage form incorporating phase change materials to protect concrete in cold weather. *Renew. Energy* **2020**, *149*, 1424–1433. [CrossRef]
42. Zhu, C.; Zhao, C.; Chen, Z.; Zhu, R.; Sheng, N.; Rao, Z. Anisotropically thermal transfer improvement and shape stabilization of paraffin supported by SIC-coated biomass carbon fiber scaffolds for thermal energy storage. *J. Energy Storage* **2022**, *46*, 103866. [CrossRef]
43. Su, H.; Guo, X.; Chen, G.; Zhang, Q.; Huang, D.; Zhang, J. A novel honeycomb-like porous carbon from loofah sponge for form-stable phase change materials with high encapsulation capacity and reliability. *Mater. Lett.* **2022**, *308*, 131118. [CrossRef]
44. Ji, X.; Liu, P.; Qiu, C.; Weng, L.; Hu, J.; Wei, R.; Zhang, Y.; Sun, W.; Guo, X. Plastic composite of bamboo charcoal stabilized polyethylene glycol with thermal energy storage and temperature regulation for building energy efficiency. *Polym. Compos.* **2024**, *45*, 1910–1921. [CrossRef]
45. Ye, P.; Liu, Z.; Jin, C.; Jin, Q.; Zhang, Q.; Luo, T.; Gui, C. Preparation and characterization of novel phase-change concrete based on different porous phase-change aggregates: Comprehensive comparison of various phase change composites. *Constr. Build. Mater.* **2024**, *439*, 137366. [CrossRef]
46. Shang, M.; Li, J.; Tian, L.; Huang, P.; Li, X.; Yu, J.; Zhang, S.; Miao, W.; Peng, J. Thermal conductivity enhancement of polyethylene glycol/NF composite as stabilized phase change materials for thermal energy storage. *J. Energy Storage* **2024**, *99*, 113313. [CrossRef]
47. Jin, J.; Liu, S.; Gao, Y.; Liu, R.; Huang, W.; Wang, L.; Xiao, T.; Lin, F.; Xu, L.; Zhang, J. Fabrication of cooling asphalt pavement by novel material and its thermodynamics model. *Constr. Build. Mater.* **2021**, *272*, 121930. [CrossRef]
48. Nam, J.; Yang, S.; Yun, B.Y.; Kim, S. Evaluation of thermal/morphological performance of SSPCM based nanoclay: Influence of the interlayer microstructure of hydrophilic and hydrophobic. *Sol. Energy Mater. Sol. Cells* **2022**, *235*, 111479. [CrossRef]
49. Zhang, Y.; Sang, G.; Du, X.; Cui, X.; Zhang, L.; Zhu, Y.; Guo, T. Development of a novel alkali-activated slag-based composite containing paraffin/ceramsite shape stabilized phase change material for thermal energy storage. *Constr. Build. Mater.* **2021**, *304*, 124594. [CrossRef]
50. Li, X.; Wei, H.; Lin, X.; Xie, X. Preparation of stearic acid/modified expanded vermiculite composite phase change material with simultaneously enhanced thermal conductivity and latent heat. *Sol. Energy Mater. Sol. Cells* **2016**, *155*, 9–13. [CrossRef]
51. Luo, M.; Song, J.; Ling, Z.; Zhang, Z.; Fang, X. Phase change material coat for battery thermal management with integrated rapid heating and cooling functions from −40 °C to 50 °C. *Mater. Today Energy* **2021**, *20*, 100652. [CrossRef]
52. Liu, X.; Chen, X.; Yang, L.; Chen, H.; Tian, Y.; Wang, Z. A review on recent advances in the comprehensive application of rice husk ash. *Res. Chem. Intermed.* **2016**, *42*, 893–913. [CrossRef]
53. Liu, C.; Zhang, W.; Liu, H.; Lin, X.; Zhang, R. A compressive strength prediction model based on the hydration reaction of cement paste by rice husk ash. *Constr. Build. Mater.* **2022**, *340*, 127841. [CrossRef]
54. Diaz, A.; Bueno, S.; Villarejo, L.; Quesada, D. Improved strength of alkali activated materials based on construction and demolition waste with addition of rice husk ash. *Constr. Build. Mater.* **2024**, *413*, 134823. [CrossRef]

55. *JTG 3430-2020*; Test Methods of Soils for Highway Engineering. Ministry of Transport of the People's Republic of China: Beijing, China, 2020.
56. Huang, W.; Zhang, J.; Wang, J.; Zheng, Y.; Ma, J.; Ding, F. Performance analysis of paraffin microcapsules and phase change concrete based on microporous cenospheres. *Constr. Build. Mater.* **2023**, *409*, 134030. [CrossRef]
57. *ASTM D6103*; Standard Test Method for Flow Consistency of Controlled Low Strength Material (CLSM). American Society of Testing Materials: West Conshohocken, PA, USA, 2017.
58. *JGJ/T 70-2009*; Standard for Test Method of Basic Properties of Construction Mortar. Ministry of Housing and Urban-Rural Development of the People's Republic of China: Beijing, China, 2009.